Supporting Information

Exposed facets dictate microbial methylation potential of mercury sulfide nanoparticles

Li Tian[1], Wenyu Guan[1], Yunyun Ji[1], Xin He[1], Wei Chen[1], Pedro J. J. Alvarez[2], Tong Zhang[1] *

1. *College of Environmental Science and Engineering, Ministry of Education Key Laboratory of Pollution Processes and Environmental Criteria, Tianjin Key Laboratory of Environmental Remediation and Pollution Control, Nankai University, 38 Tongyan Rd., Tianjin 300350, China*
2. *Department of Civil and Environmental Engineering, Rice University, 6100 Main Street, Houston, TX 77005, USA*

* Corresponding author: zhangtong@nankai.edu.cn

Methods

Precipitation of mercury sulfide (HgS) in the presence of natural ligands. The inorganic mercury (Hg) stock solution consisted of $Hg(NO_3)_2$ (Sinopharm, China) dissolving in 0.02 M trace-metal grade HNO_3. Na_2S stocks were prepared by dissolving freshly washed and dried crystals of $Na_2S \cdot 9H_2O$ (Aladdin, China) in N_2-purged nanopure water (>18 MΩ-cm), and were utilized within 4 h of preparation. Standard materials of natural organic matter (NOM), including Suwannee River humic acid (SRHA, catalog number: 3S101H) and Suwannee River fulvic acid (SRFA, catalog number: 2S101F), were purchased from International Humic Substances Society (IHSS, USA). The NOM stock solution was prepared by dissolving the NOM powder in nanopure water with pH adjusted to 7.5 using 0.01 M NaOH. The NOM stock solution was kept refrigerated, and filtered through 0.2-μm syringe filters and the filtrate was quantified using combustion catalytic oxidation/infrared spectroscopy (Multi N/C 3100 TOC, Analytik Jena AG, Germany) prior to use. The powder stock of low-molecular-weight (LMW) thiol ligand, glutathione (GSH, Aladdin, China), was kept refrigerated prior to dissolving in N_2-purged nanopure water. The stock solution of GSH was freshly prepared for each precipitation experiment and discarded after use.

The buffer solution for the precipitation experiments contained 0.01 M $NaNO_3$ and 4 mM sodium 4-(2-hydroxyethyl) piperazine-1-ethanesulfonate (HEPES) with pH adjusted to 7.2 and then double-filtered to <0.05 μm. In this buffer solution, 50 μM $Hg(NO_3)_2$ and

50 μM Na_2S were mixed with 10 mg-C l^{-1} SRHA or SRFA; 60 μM $Hg(NO_3)_2$ and 60 μM Na_2S were mixed with 100 μM GSH. The precipitation products were collected after 1-d, 11-d and 21-d aging period (in dark, at room temperature, 23-26℃), respectively, and utilized for material characterization and microbial methylation experiments. Precipitation experiments of $Hg(NO_3)_2$ and Na_2S in the same buffer solution without natural ligands were also conducted and the precipitation products were included in the aging experiments as control samples.

Preparation of model HgS nanoparticles. Model HgS nanoparticles with different exposed facets were synthesized following previously established methods[1]. For synthesizing model nanoparticles I, 1.6 g $Hg(CH_3COO)_2 \cdot 2H_2O$ and 0.5 g thiourea (Aladdin, China) were mixed in 100 ml nanopure water and pH was adjusted to 4.0 using acetic acid. Then 0.5 g Polyvinylpyrrolidone (PVP, Mw 40 kD, Amresco, USA) was added to the suspension, which was sonicated for 30 min while purged with nitrogen. The black-colored precipitates were collected from the suspension using centrifugation and then thoroughly washed with absolute ethanol and nanopure water. Finally, the precipitates were heated at 300℃ for 2 h in the pipe furnace to remove the residual PVP. The procedure for preparing model nanoparticles II was the same as that of nanoparticles I, except that no PVP was added to the experimental suspension. After synthesis, the total carbon content in the model materials were measured on a TOC analyzer (Multi N/C

41 3100 TOC, Analytik Jena AG, Germany), and appeared to be 2.6% and 2.8% of the total
42 particle mass for model material I and II, respectively, indicating minimal residual PVP
43 on model nanoparticles I. The two model materials were freeze-dried and stored in an
44 anaerobic chamber with desiccants prior to material characterization and microbial
45 methylation experiments.
46
47 **Characterization of HgS nanoparticles.** The particle morphology of the products of
48 HgS precipitation experiments and the synthesized model nanoparticles were analyzed
49 using transmission electron microscopy coupled with energy dispersive X-ray
50 spectroscopy (TEM-EDX, JEM-2100, JEOL, Japan). Samples for TEM analysis were
51 prepared by depositing droplets of the particle suspensions on 200-mesh carbon-coated
52 copper grids, and allowing the grids to air dry in an anaerobic chamber. For each type of
53 HgS nanoparticle, the geometric diameters were obtained by measuring 100 particles
54 from the TEM images using image processing software Image J, based on which the
55 geometric surface areas were calculated by assuming spherical particles with a density of
56 7.71 g cm^{-3} (ref. [2,3]). The crystallographic structures of the HgS nanoparticles were
57 analyzed by X-ray diffraction (XRD) spectroscopy on a Rigaku diffractometer (Ultima
58 IV, Rigaku Inc., Japan) with Cu Kα radiation (λ = 1.5418 Å). The crystallite diameters
59 were calculated according to the Scherrer formula using the XRD data[4]. High-resolution
60 TEM (HR-TEM) was utilized to assess the lattice spacing of the crystalline nanoparticles

to further corroborate the crystalline phases determined by XRD analysis. The surface elemental composition of HgS nanoparticles were characterized with X-ray photoelectron spectrometry (XPS, Axis Ultra DLD, Kratos, Britain). The hydrodynamic diameters and zeta potential of nanoparticle aggregates were analyzed on a Zetasizer (Nano Series ZS90, Malvern, USA)

Microbial methylation experiments. Methylating bacterium *Desulfovibrio desulfuricans* ND132 was cultured in Hungate tubes (Changshu Wente experimental ware co. LTD, China), which were kept in dark and at room temperature (23-26℃) in an anaerobic chamber. The bacterial cultures were grown in sulfate-containing media and then transferred in fermentative media twice before mercury methylation experiments. The sulfate-containing media and fermentative media were prepared according to previously reported methodologies, and contain the redox sensitive resazurin as well as the reductant Ti-nitrilotriacetic acid (NTA) to help maintain anaerobic conditions[5,6]. The inoculation ratio for the test cultures were 1:37 and 1:30 in the methylation experiments examining the bioavailability of the aged HgS precipitation products and the model nanoparticles, respectively.

Prior to the addition of HgS nanoparticles, *D. desulfuricans* ND132 was pre-cultured to reach late-log growth phase. The stock suspensions of model nanoparticles I and II were prepared by adding the corresponding powder products into nanopure water, which

were sonicated for 120 min in anaerobic vials before taking aliquots. The total mercury addition for the methylation experiments of model nanoparticles and precipitation products was 50 nM and 10 nM, respectively. The pH of the test cultures was maintained at 7.0-7.3 using 3-(N-morpholino) propanesulfonic acid (MOPS). The test cultures were placed in dark, at room temperature (23-26°C) in an anaerobic chamber during the entire time course of the methylation experiments. Two sets of controls were incubated under the same conditions including (1) uninoculated media spiked with $Hg(NO_3)_2$; (2) bacterial cultures without mercury addition. MeHg production in all control samples were below the detection limit (≤0.09 pM MeHg) and thus abiotic methylation and mercury contamination were negligible in our experiments. At each time point, triplicate vials were collected and aliquots were taken for quantification of cell numbers using flow cytometry (Accuri C6 Plus, BD, Singapore) after the bacterial cells were stained with SYBR Green I (Life Technologies, USA). Total mercury concentrations were measured using cold vapor atomic fluorescence spectrometry (CVAFS, Tekran 2600, Tekran, USA)[7]. Afterward, the rest of the cultures were preserved by 0.4% (v/v) trace-metal-grade HCl and kept refrigerated prior to methylmercury (MeHg) analysis. MeHg concentrations were quantified by distillation, aqueous phase ethylation, gas chromatographic separation, and CVAFS (Tekran 2700, Tekran, USA)[8].

Mercury methylation bioassays were also carried out in the presence of divalent zinc, Zn(II). The Zn(II) stock solutions were prepared by dissolving trace-metal grade

$ZnCl_2$ (Acros Organics, Belgium) in 0.01 M trace-metal grade HCl using degassed nanopure water. Zn(II) was injected into the cultures of *D. desulfuricans* ND132 to reach final concentrations of 100-500 μM, before exposure to 10 nM HgS nanoparticles co-precipitated with GSH and aged for 1 d. The rest of the protocols were consistent with the other mercury methylation experiments conducted in this research.

Characterization of nanoparticle−cell association. In a subset of test cultures exposed to model nanoparticles I and II, bacterial cells with cell-bound nanoparticles were separated from unassociated nanoparticles by a density gradient centrifugation method using OptiPrep™ kit (Alere Technologies AS, Oslo, Norway)[9]. Briefly, bacterial cells with bound and unbound nanoparticles were harvested by centrifugation at 9,000 rpm for 5 min. The pellets were resuspended in 1.5 ml of 50% (w/v) OptiPrep™ medium and then centrifuged at 9,000 rpm for 5 min. Afterward, the top fraction (0.7 ml total) was used for quantification of cell-bound mercury, which was normalized with the cell numbers measured before centrifugation. The cell recovery during this procedure was assessed by measuring the protein content before and after gradient centrifugation using the bicinchoninic acid (BCA) assay[10], and was found to be 93.9 ± 6.4%.

In a subset of test cultures exposed to HgS nanoparticles co-precipitated with SRHA, SRFA or GSH, samples were collected for TEM analysis by centrifugation. The pellets were washed with 10 mM phosphate buffered saline (PBS, pH 7.4), resuspended

in a fixative solution containing 2.5% (v/v) glutaraldehyde, and stored at 4℃ overnight. The cells were washed with PBS again before and after being fixed in 1% (w/v) osmium tetroxide. Then the samples were dehydrated with 30%-100% (v/v) ethanol, embedded in Epon812 epoxy resin, and cured at 37℃, 45℃ and 65℃ for 24 h, respectively. Subsequently, they were sliced into ultra-thin sections by the UltracutE microtome. These sections were deposited on 200-mesh carbon-coated copper grids and analyzed by TEM (JEM-1200EX, JEOL, Japan) and EDX (OXFOR MAX80, Oxford Instruments, Britain).

Molecular dynamics (MD) simulations. The protein sequence and three-dimensional structure of periplasmic solute-binding protein of zinc transport system of *D. desulfuricans* ND132, ZnuA, was obtained from UniProt database (https://www.uniprot.org/uniprot/F0JJA9) and predicted by ITASSER online service[11-13]. The crystal structure of metacinnabar was taken from the website of https://materialsproject.org/materials/mp-1123/. The spherical structures of facet (111), (220) and (311) were constructed by the software module of biovia material studio 2017. All of the MD calculations were carried out using the GROMACS 5.0.4 package[14-16] in the NPT ensemble. The protein force field was performed using Amber 99SB-ILDN all-atoms force field[17]. The parameters of the facets were taken from the literature[18] and generated by the x2top command in GROMACS.

MD simulation was performed from 0 to 100 ns for each calculation. The temperature was stabilized at 298 K by Nose Hoover thermostat coupling[19]. The cut-off switching function for calculating the non-bonded van der Waals interactions started at 1.2 nm and reached zero at 1.35 nm. The long-range electrostatic interaction was calculated by Particle mesh Ewald[20] summation, with a truncation radius of 1.2 nm. Periodic boundary conditions were used throughout the calculation. The limitation of bond length was implemented through linear constraint solver algorithm[21]. The hydrated layers were modeled as point charge water molecules[22]. The system was kept neutral by adding chloride and sodium ions. The time step of calculated data was 2 fs. Molecular graphics and visualization were performed using the free VMD software[23].

Adsorption of natural ligands to model nanoparticles. Adsorption experiments were performed in a series of 40 ml EPA vials containing 0.01 M $NaNO_3$. SRHA, SRFA or GSH with an initial concentration of 10 mg-C l^{-1}, 10 mg-C l^{-1} or 100 mg l^{-1} was added to the vials that contain 1,000 mg l^{-1} model nanoparticles I or II, respectively. For all the adsorption experiments, pH of the reaction matrices was adjusted to 7.0 ± 0.7 using HNO_3 and NaOH. The vials were then kept at room temperature (23-26°C) on a rotating mixer at a speed of 70 rpm min^{-1}. Two sets of controls were incubated under the same conditions including (1) HgS nanoparticles with no ligands; (2) SRHA, SRFA or GSH with no nanoparticles. At each time point, triplicate vials were sacrificed and centrifuged

160 at 12,000 rpm for 3 min, which effectively separated the adsorbed ligands from free
161 ligands according to the controls (i.e., <2% HgS nanoparticles and >99% ligands
162 remained in the supernatant after centrifugation). The supernatant was sampled to
163 determine the concentration of the unadsorbed SRHA, SRFA or GSH and the amount of
164 the adsorbed ligands were calculated using a mass balance approach. The concentrations
165 of SRHA and SRFA were measured on a TOC analyzer (Multi N/C 3100 TOC, Analytik
166 Jena AG, Germany), and the GSH concentrations were quantified with Total Amino Acid
167 Assay Kit (Nanjing Jiancheng Bioengineering Institute, China) by following the
168 manufacturer's protocols.
169
170 **Density functional theory (DFT) analysis.** The adsorption of GSH on the (111), (220)
171 and (311) facets of metacinnabar was simulated using DFT analysis conducted by the
172 Vienna Ab-initio Simulation Package (VASP). The electron-ion interaction was assessed
173 by the method of projector-augmented wave and the cutoff value of the plane-wave was
174 420 eV. The Perdew-Burke-Ernzerh (PBE)[24-26] method was used for the description of the
175 exchange and correlation potential, with spin polarization considered in all computations.
176 The electronic structure calculations were employed with a Gaussian smearing of 0.1 eV,
177 and 1 × 1 × 1 Monkhorst-Pack k-point grids were used for the sampling of the Brillouin
178 zone[27].

We used a (3 × 3) repeated unit cell with a four-layer slab for the (111), (220) and (311) surfaces for GSH adsorption. All slabs were spaced more than 14 Å perpendicular to the slab surface to avoid artificial interaction due to periodicity. During optimization, the atoms of the two layers at the bottom were fixed, and the remaining atoms were relaxed to reach stable configurations. Atoms were optimized until the residual forces were below 0.02 eV $Å^{-1}$. The adsorption energies are estimated using the equation:

$$E_{ads}A = E_{slab+A} - E_{slab} - E_A \quad (1)$$

where $E_{ads}A$ is the interaction energy between slab fragment and molecule fragment in the optimized configurations; E_{slab+A} is the total energy of the slab and the molecule in the optimized configurations; E_{slab} is the energy of the slab alone in the optimized configurations; E_A is the energy of the molecule alone in the optimized configurations.

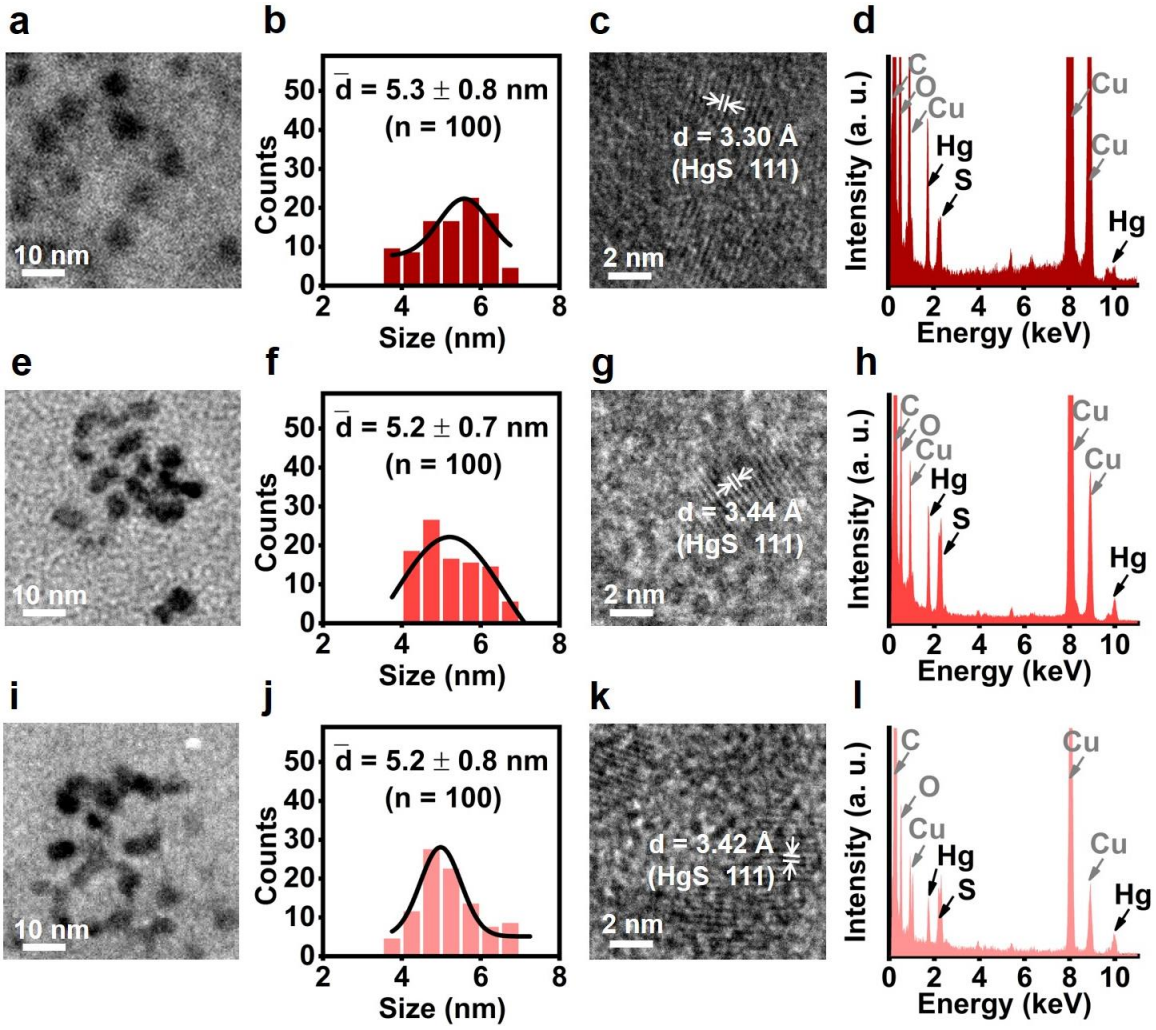

Supplementary Figure 1. TEM images (a, e, i), particle size distribution (b, f, j), high-resolution TEM images (c, g, k) and EDX spectra (d, h, l) of HgS nanoparticles formed in the presence of SRHA, aged for 1 d (a-d), 11 d (e-h) and 21 d (i-l). Values of particle sizes represent mean ± 1 SD of one hundred samples.

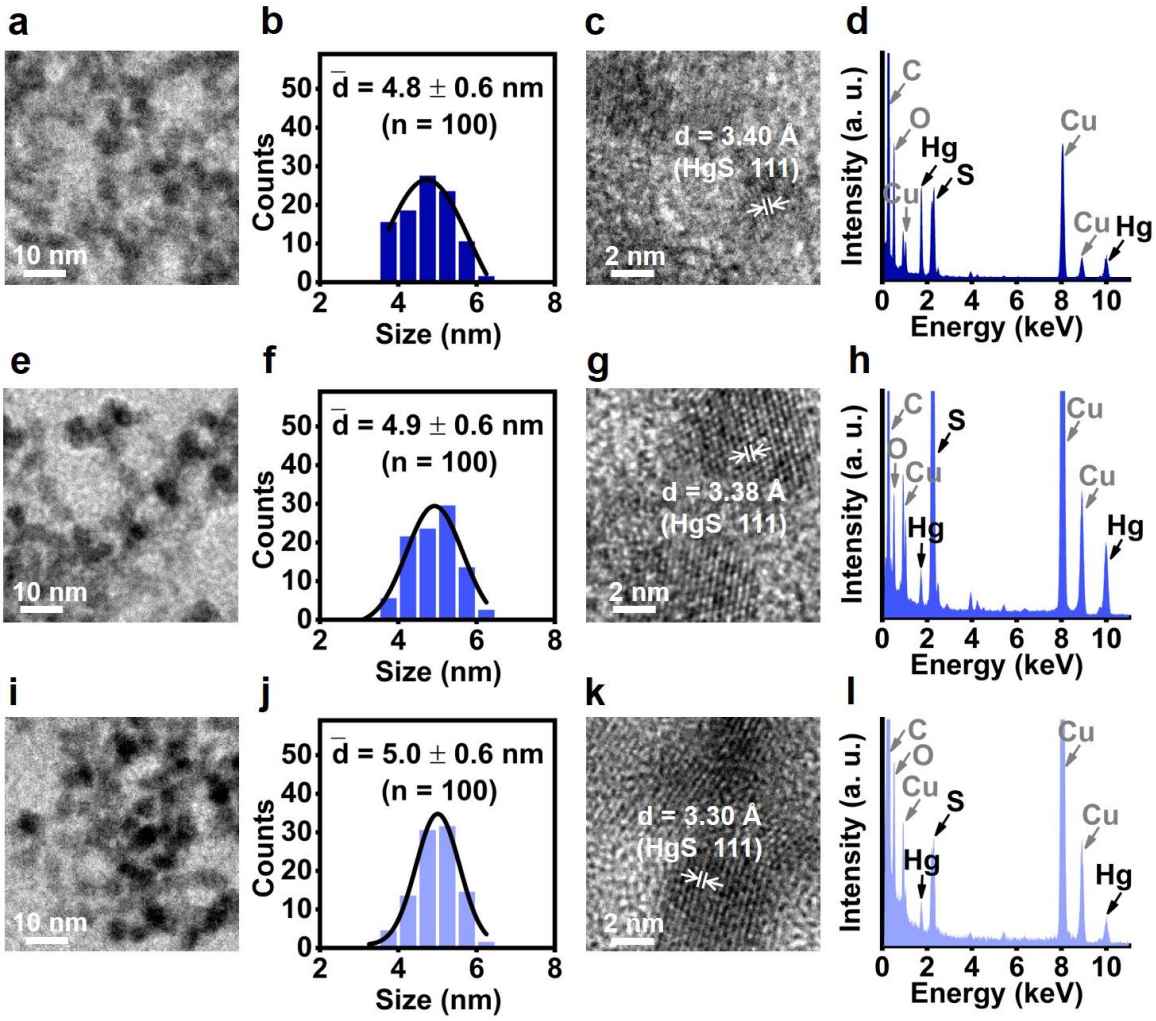

Supplementary Figure 2. TEM images (a, e, i), particle size distribution (b, f, j), high-resolution TEM images (c, g, k) and EDX spectra (d, h, l) of HgS nanoparticles formed in the presence of SRFA, aged for 1 d (a-d), 11 d (e-h) and 21 d (i-l). Values of particle sizes represent mean ± 1 SD of one hundred samples.

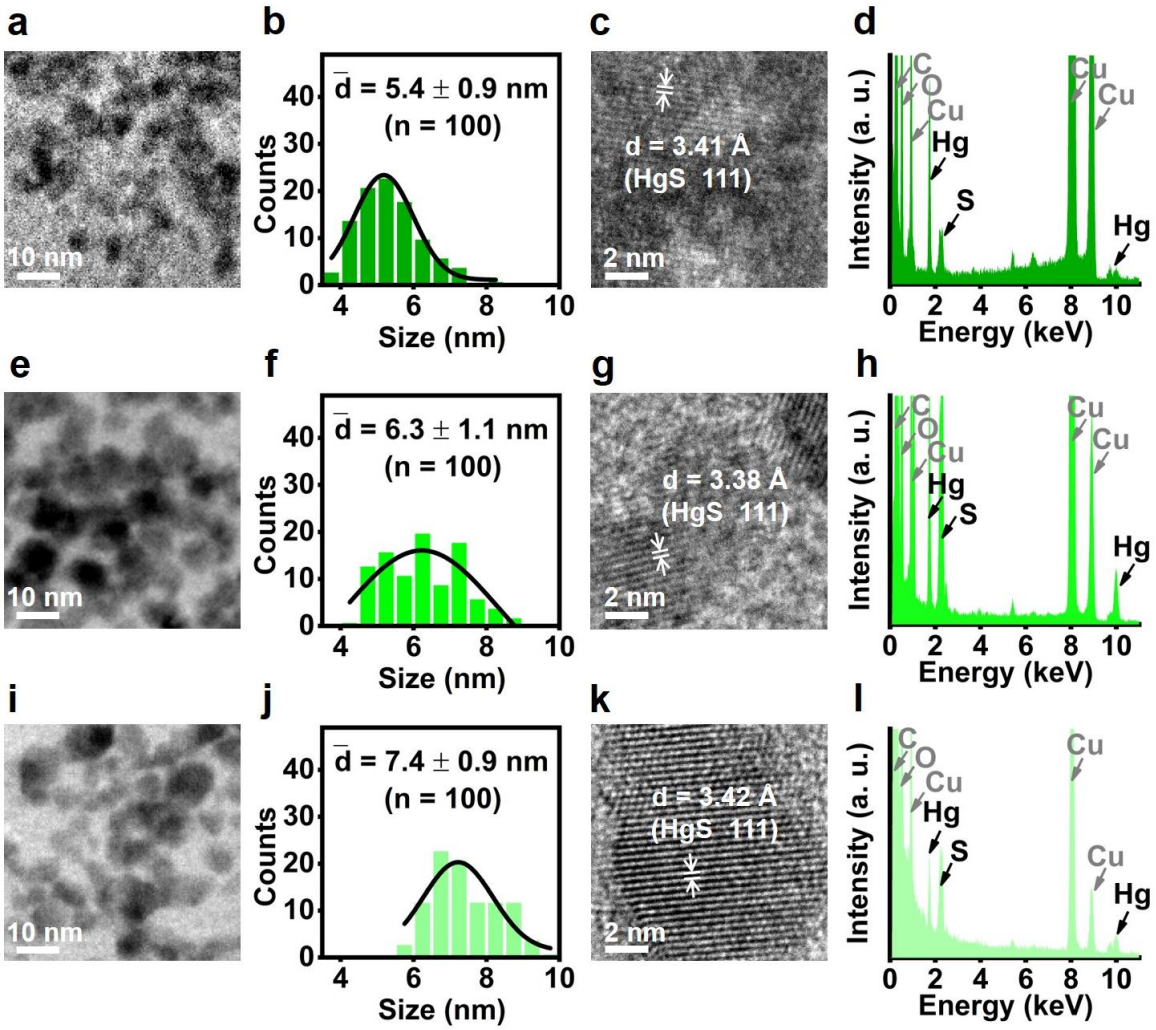

Supplementary Figure 3. TEM images (a, e, i), particle size distribution (b, f, j), high-resolution TEM images (c, g, k) and EDX spectra (d, h, l) of HgS nanoparticles formed in the presence of GSH, aged for 1 d (a-d), 11 d (e-h) and 21 d (i-l). Values of particle sizes represent mean ± 1 SD of one hundred samples.

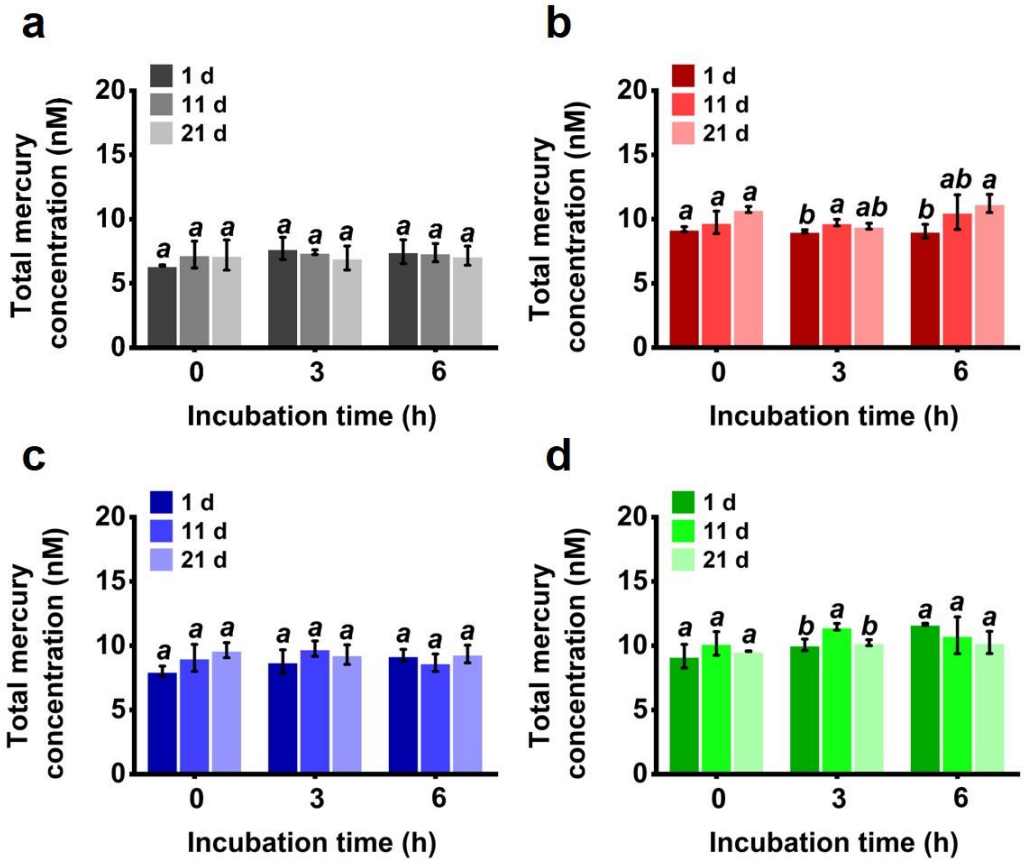

Supplementary Figure 4. Total mercury concentrations in methylating bacterial cultures exposed to HgS formed in the absence of natural ligands (a), and in the presence of SRHA (b), SRFA (c) or GSH (d). Values that are statistically different (p <0.05) among treatments according to the one-way ANOVA are indicated by italic lowercase letters. Error bars represent ± 1 SD of triplicate samples.

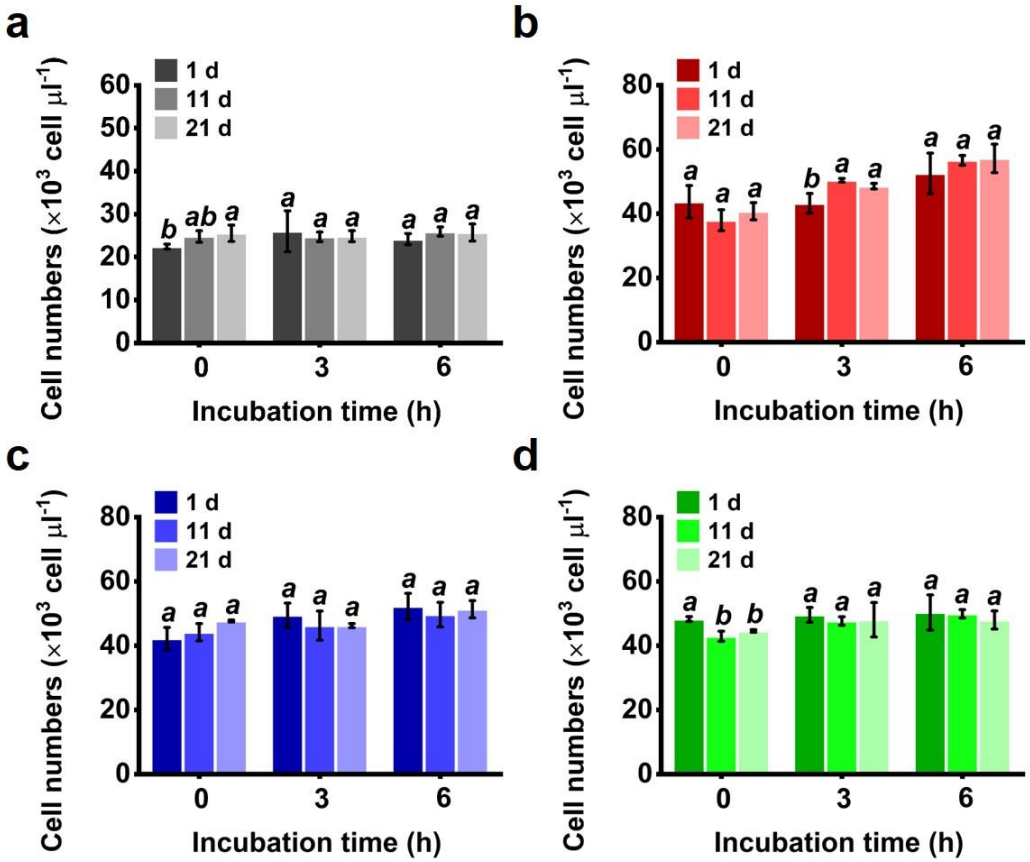

Supplementary Figure 5. Total cell number concentrations in methylating bacterial cultures exposed to HgS formed in the absence of natural ligands (a), and in the presence of SRHA (b), SRFA (c) or GSH (d). Values that are statistically different (p <0.05) among treatments according to the one-way ANOVA are indicated by italic lowercase letters. Error bars represent ± 1 SD of triplicate samples.

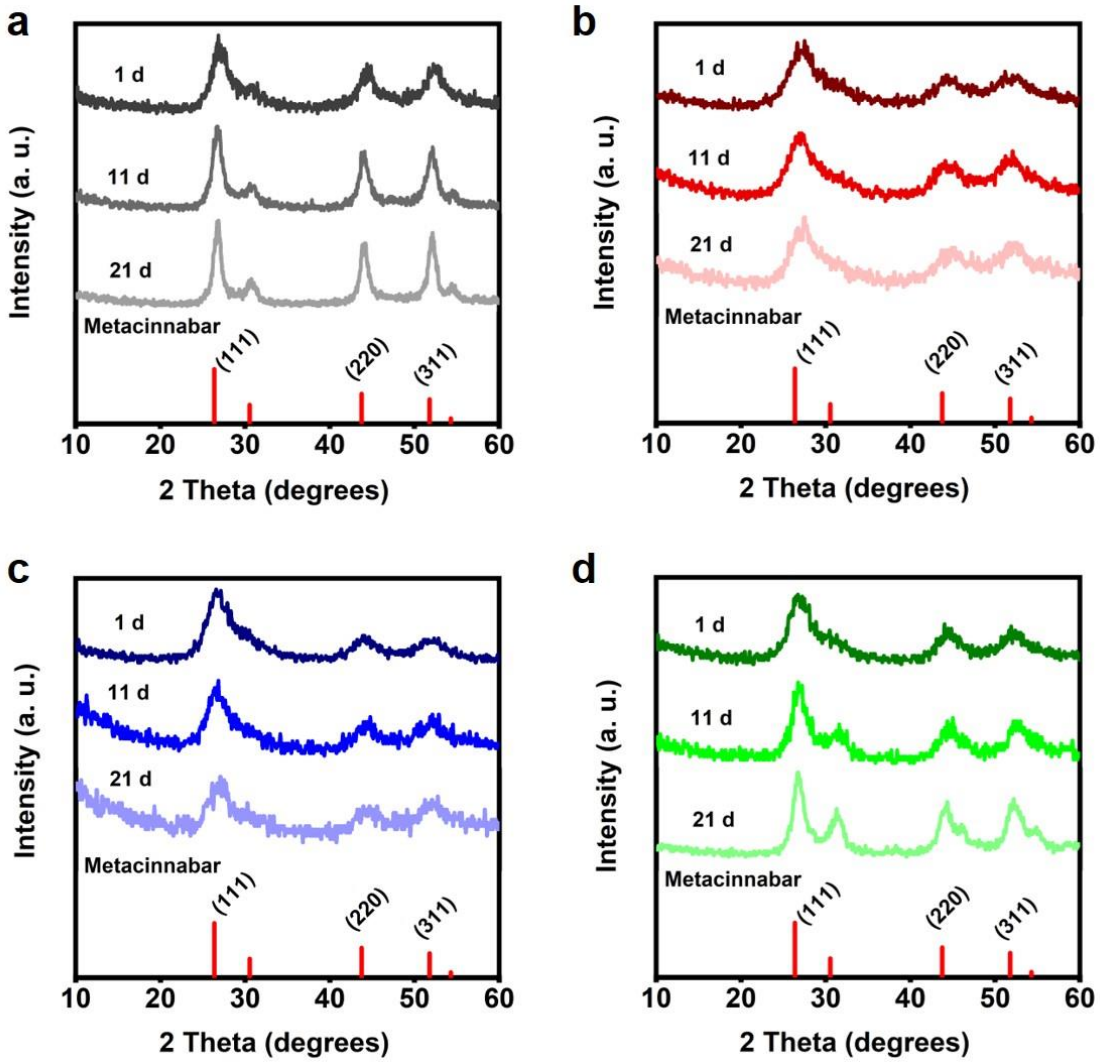

Supplementary Figure 6. XRD spectra of HgS formed in the absence of natural ligands (a), and in the presence of SRHA (b), SRFA (c) or GSH (d).

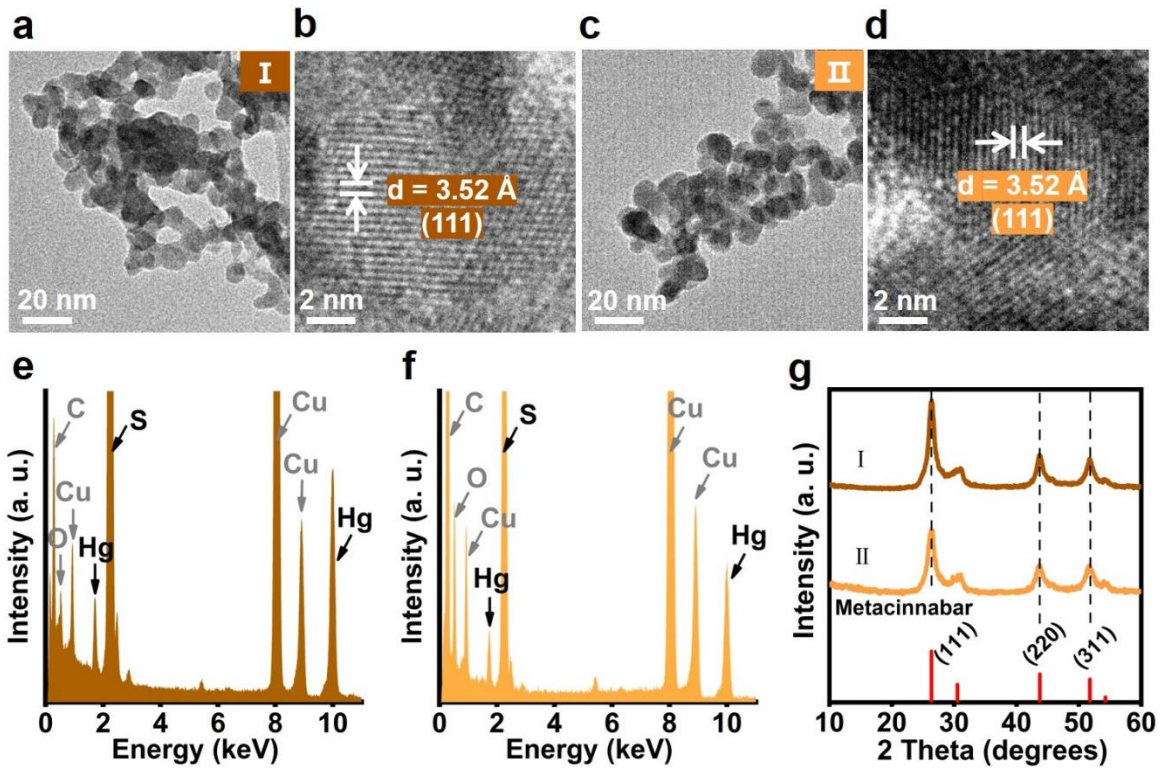

Supplementary Figure 7. TEM images (a, c), high-resolution TEM images (b, d), EDX spectra (e, f) and XRD spectra (g) of model material I (a, b, e, g) and II (c, d, f, g).

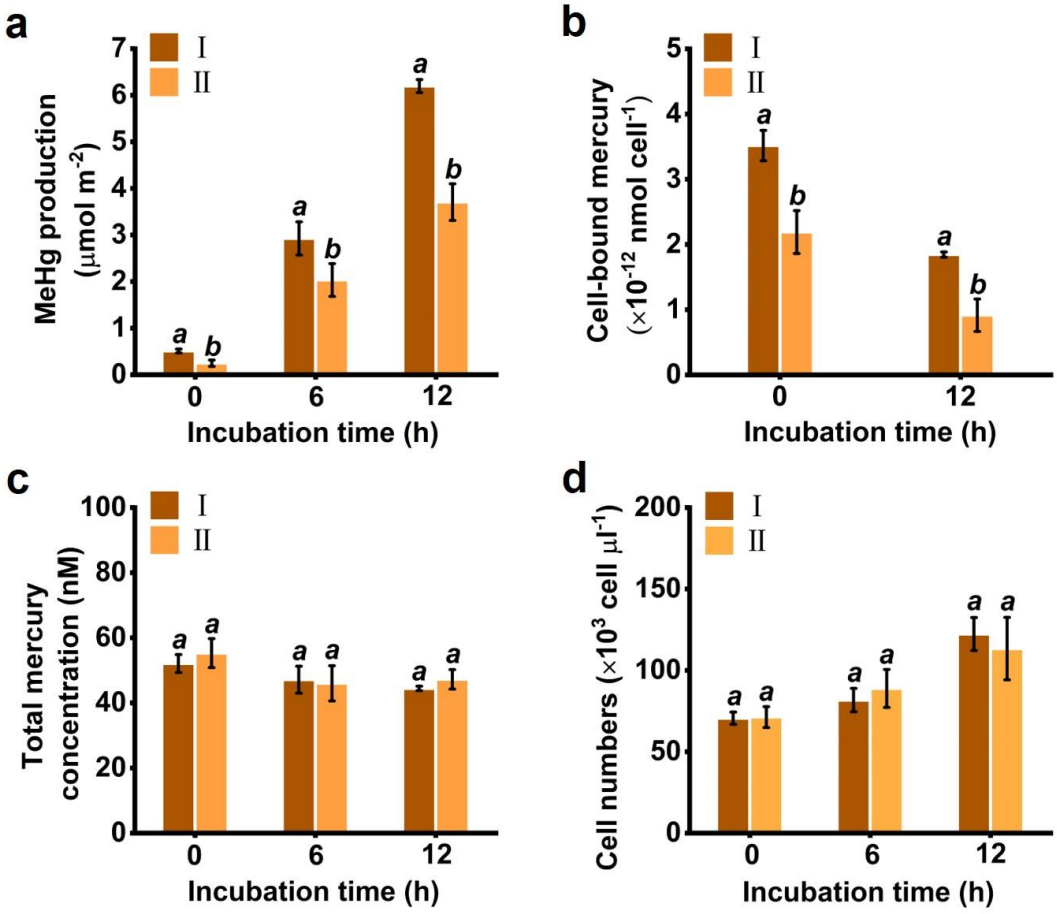

Supplementary Figure 8. Concentrations of microbially produced MeHg (a), cell-bound mercury (b), total mercury (c) and total cell number (d) in cultures of *D. desulfuricans* ND132 exposed to 50 nM model material I and II. Values that are statistically different (p <0.05) between treatment I and II according to the independent t-test are indicated by italic lowercase letters. Error bars represent ± 1 SD of triplicate samples.

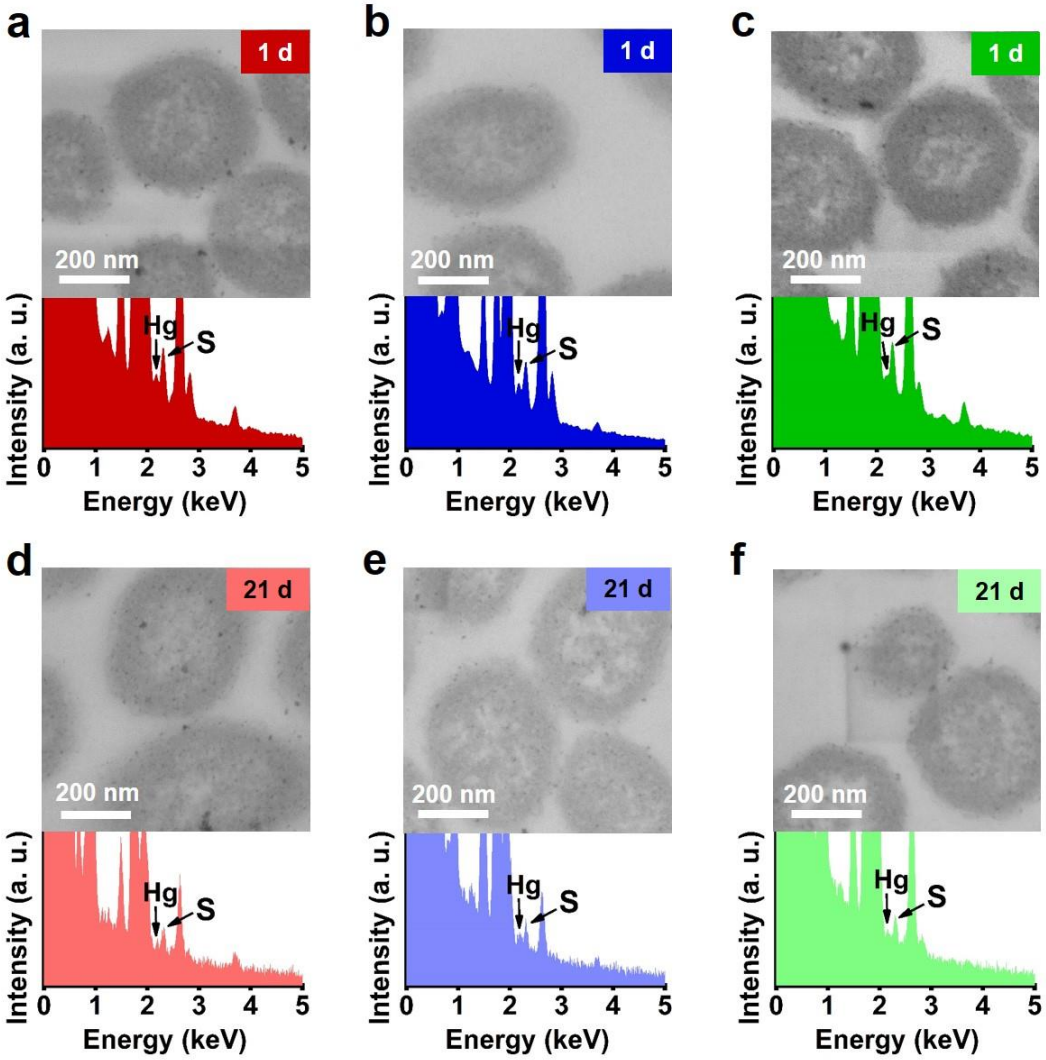

Supplementary Figure 9. TEM images and EDX spectra of the thin sections of *D. desulfuricans* ND132 after exposure to HgS nanoparticles formed in the presence of SRHA (a, d), SRFA (b, e) or GSH (c, f), aged for 1 d (a-c) or 21 d (d-f).

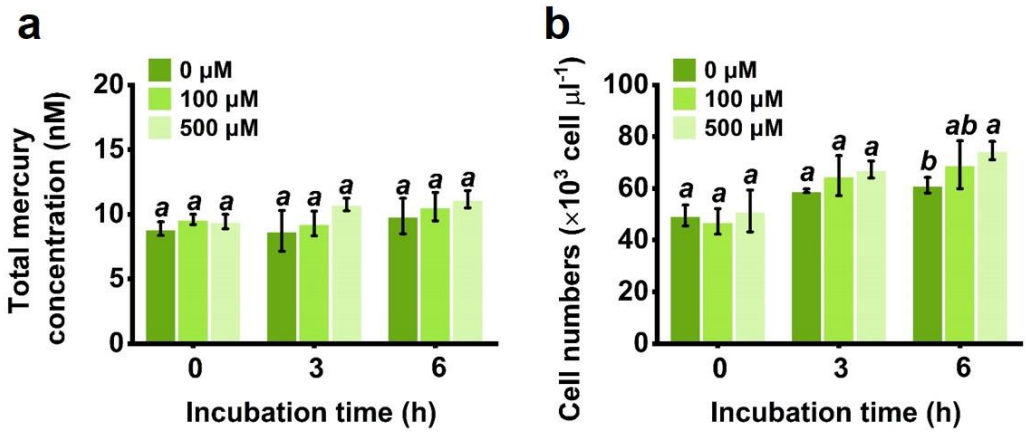

Supplementary Figure 10. Concentrations of total mercury and total cell number in cultures of *D. desulfuricans* ND132 exposure to Zn(II) and HgS nanoparticles formed in the presence of GSH and aged for 1 d. Values that are statistically different (p <0.05) among different treatments according to the one-way ANOVA are indicated by italic lowercase letters. Error bars represent ± 1 SD of triplicate samples.

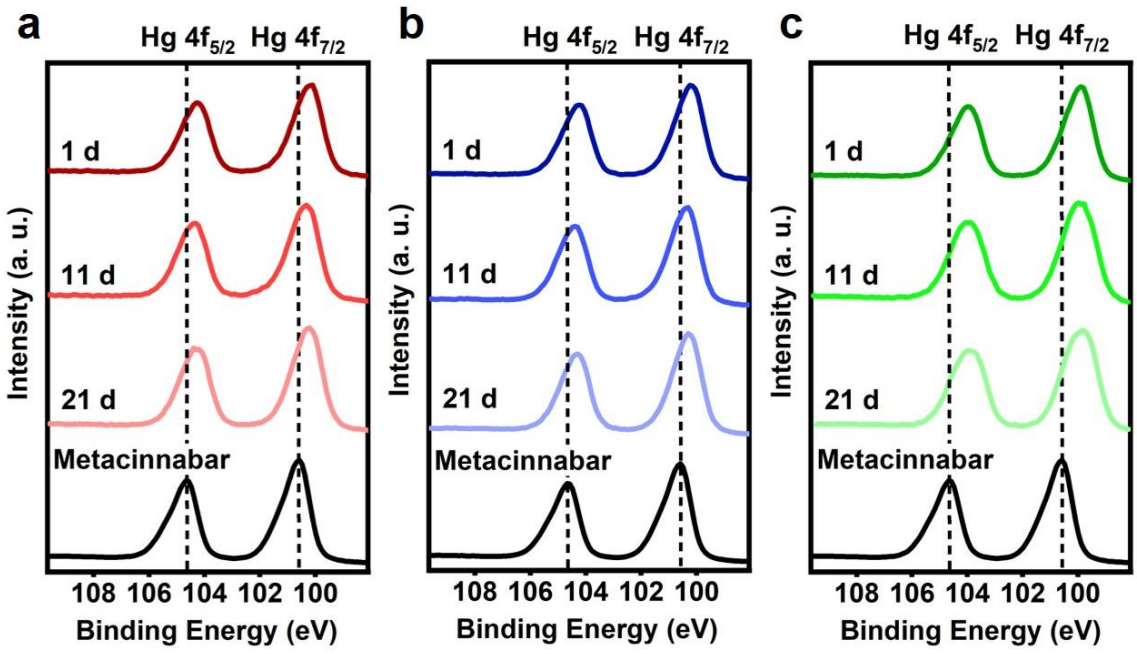

Supplementary Figure 11. Hg 4f XPS spectra of HgS nanoparticles formed in the presence of SRHA (a), SRFA (b) or GSH (c).

Supplementary Table 1. Physicochemical properties of HgS nanoparticles formed in the presence of natural ligands.

Physicochemical properties	Aging time (d)	Ligand		
		SRHA	SRFA	GSH
Geometric diameter (nm)*	1	5.3 ± 0.8^{a}	4.8 ± 0.6^{a}	5.4 ± 0.9^{c}
	11	5.2 ± 0.7^{a}	4.9 ± 0.6^{a}	6.3 ± 1.1^{b}
	21	5.2 ± 0.8^{a}	5.0 ± 0.6^{a}	7.4 ± 0.9^{a}
Geometric surface area (m^2 g^{-1})*	1	151 ± 26^{a}	165 ± 21^{a}	149 ± 24^{a}
	11	152 ± 21^{a}	162 ± 23^{a}	127 ± 22^{b}
	21	152 ± 23^{a}	159 ± 19^{a}	106 ± 13^{c}
Crystallite diameter (nm)†	1	3.0 ± 0.4^{a}	3.3 ± 0.4^{b}	3.8 ± 0.2^{c}
	11	3.1 ± 0.4^{a}	3.9 ± 0.2^{b}	4.6 ± 0.4^{b}
	21	3.6 ± 0.4^{a}	4.5 ± 0.2^{a}	6.0 ± 0.4^{a}
Hydrodynamic diameter (nm)†	1	482 ± 60^{a}	52.9 ± 1.5^{b}	388 ± 33^{b}
	11	441 ± 53^{a}	55.3 ± 18^{b}	570 ± 69^{ab}
	21	537 ± 189^{a}	78.6 ± 2.7^{a}	623 ± 161^{a}
Zeta potential (mV)†	1	-23.2 ± 0.8^{a}	-26.0 ± 0.5^{ab}	-23.4 ± 4.3^{a}
	11	-23.1 ± 1.0^{a}	-26.9 ± 1.6^{a}	-21.3 ± 0.5^{a}
	21	-23.6 ± 0.4^{a}	-23.4 ± 1.9^{b}	-23.3 ± 0.9^{a}

*Values represent mean ± 1 SD of one hundred samples. Values that are statistically different (p <0.05) among the treatments with different aging time according to the one-way ANOVA are indicated by italic lowercase letters.

†The crystallite diameters are calculated according to the Scherrer formula[4] using the XRD data (Supplementary Figure 6). Values represent mean ± 1 SD of triplicate samples. Values that are statistically different (p <0.05) among the treatments with different aging time according to the one-way ANOVA are indicated by italic lowercase letters.

Supplementary Table 2. Physicochemical properties of model HgS nanoparticles.

Physicochemical properties	Model material I	Model material II
(111)/(220)[*]	2.4	2.0
Geometric diameter (nm)[†]	8.9 ± 1.0[a]	9.0 ± 1.2[a]
Geometric surface area (m^2 g^{-1})[†]	88.5 ± 10[a]	87.6 ± 12[a]
Crystallite diameter (nm)[‡]	6.5 ± 0.1[a]	6.5 ± 0.5[a]
Hydrodynamic diameter (nm)[‡]	599 ± 90[a]	602 ± 221[a]
Zeta potential (mV)[‡]	-12.0 ± 1.5[a]	-14.4 ± 0.2[a]

[*]The intensity ratios of the XRD diffraction peaks of metacinnabar (111) and (220) facets.

[†]Values represent mean ± 1 SD of one hundred samples. Values that are statistically different (p <0.05) between treatment I and II according to the independent *t*-test are indicated by italic lowercase letters.

[‡]The crystallite diameters are calculated according to the Scherrer formula[4] using the XRD data (Supplementary Figure 7g). Values represent mean ± 1 SD of triplicate samples. Values that are statistically different (p <0.05) between treatment I and II according to the independent *t*-test are indicated by italic lowercase letters.

References

1 Wang, H. & Zhu, J. J. A sonochemical method for the selective synthesis of α-HgS and β-HgS nanoparticles. *Ultrason. Sonochem.* **11,** 293-300 (2004).

2 Zhang, T. et al. Methylation of mercury by bacteria exposed to dissolved, nanoparticulate, and microparticulate mercuric sulfides. *Environ. Sci. Technol.* **46,** 6950-6958 (2012).

3 Institute of Experimental Mineralogy, Russian Academy of Science. Crystallographic and Crystallochemical Database for Minerals and their Structural Analogues. http://database.iem.ac.ru/mincryst/index.php (Created 1997, Updated 2020).

4 Birks, L. S. F., H. Particle size determination from X-ray line broadening. *J. Appl. Phys.* **17,** 687-691 (1946).

5 Benoit, J. M., Gilmour, C. C. & Mason, R. P. Aspects of bioavailability of mercury for methylation in pure cultures of *Desulfobulbus propionicus* (1pr3). *Appl. Environ. Microbiol.* **67,** 51-58 (2001).

6 Gilmour, C. C. et al. Sulfate-reducing bacterium *Desulfovibrio desulfuricans* ND132 as a model for understanding bacterial mercury methylation. *Appl. Environ. Microbiol.* **77,** 3938-3951 (2011).

7 U.S. Environmental Protection Agency. Method 1631, Revision D: Mercury in Water by Oxidation, Purge and Trap, and Cold Vapor Atomic Fluorescence Spectroscopy. (Washington, DC, 2001).

8 U.S. Environmental Protection Agency. Method 1630: Methyl Mercury in water by Distillation, Aqueous Ethylation, Purge and Trap, and CVAFS. (Washington, DC, 2001).

9 Mortimer, M., Petersen, E. J., Buchholz, B. A., Orias, E. & Holden, P. A. Bioaccumulation of multiwall carbon nanotubes in tetrahymena thermophila by direct feeding or trophic transfer. *Environ. Sci. Technol.* **50,** 8876-8885 (2016).

10 Smith, P. K. et al. Measurement of protein using bicinchoninic acid. *Anal. Biochem.* **150,** 76-85 (1985).

11 Roy, A., Kucukural, A. & Zhang, Y. I-TASSER: a unified platform for automated protein structure and function prediction. *Nat. Protoc.* **5,** 725-738 (2010).

12 Yang, J. et al. The I-TASSER Suite: protein structure and function prediction. *Nat. Methods* **12,** 7-8 (2015).

13 Yang, J. & Zhang, Y. I-TASSER server: new development for protein structure and function predictions. *Nucleic Acids Res.* **43,** W174-W181 (2015).

14 Abraham, M. J. et al. GROMACS: high performance molecular simulations through multi-level parallelism from laptops to supercomputers. *SoftwareX* **1-2,** 19-25 (2015).

15 Pronk, S. et al. GROMACS 4.5: a high-throughput and highly parallel open source molecular simulation toolkit. *Bioinformatics* **29,** 845-854 (2013).

16 Van der Spoel, D. et al. GROMACS: fast, flexible, and free. *J. Comput. Chem.* **26,** 1701-1718 (2005).

17 Lindorff-Larsen, K. et al. Improved side-chain torsion potentials for the Amber ff99SB protein force field. *Proteins* **78,** 1950-1958 (2010).

18 Fuchs, J. F. et al. New model potentials for sulfur-copper(I) and sulfur-mercury(II) interactions in proteins: from *ab initio* to molecular dynamics. *J. Comput. Chem.* **27,** 837-856 (2006).

19 Evans, D. J. & Holian, B. L. The Nose–Hoover thermostat. *J. Chem. Phys.* **83,** 4069-4074 (1985).

20 Tom, D., Darrin, Y. & Lee, P. Particle mesh Ewald: an *N*·log(*N*) method for Ewald sums in large systems. *J. Chem. Phys.* **98,** 10089-10092 (1993).

21 Hess, B., Bekker, H., Berendsen, H. J. C. & Fraaije, J. G. E. M. LINCS: a linear constraint solver for molecular simulations. *J. Comput. Chem.* **18,** 1463-1472 (1997).

22 Jorgensen, W. L., Chandrasekhar, J., Madura, J. D., Impey, R. W. & Klein, M. L. Comparison of simple potential functions for simulating liquid water. *J. Chem. Phys.* **79,** 926-935 (1983).

23 Humphrey, W., Dalke, A. & Schulten, K. VMD: visual molecular dynamics. *J. Mol. Graphics* **14,** 33-38 (1996).

24 Kresse, G. & Hafner, J. Ab initio molecular dynamics for liquid metals. *Phys. Rev. B* **48,** 13115-13118 (1993).

25 Kresse, G. & Furthmüller, J. Efficient iterative schemes for *ab initio* total-energy calculations using a plane-wave basis set. *Phys. Rev. B* **54,** 11169-11186 (1996).

26 Kresse, G. & Joubert, D. From ultrasoft pseudopotentials to the projector augmented-wave method. *Phys. Rev. B* **59,** 1758-1775 (1999).

27 Monkhorst, H. J. & Pack, J. D. Special points for brillouin-zone integrations. *Phys. Rev. B* **13,** 5188-5192 (1976).